Soft Matter

PAPER

View Article Online
View Journal | View Issue

Cite this: *Soft Matter*, 2016, **12**, 8124

Influence of chain topology on polymer crystallization: poly(ethylene oxide) (PEO) rings *vs.* linear chains†

George Zardalidis,[a] Julian Mars,[b] Jürgen Allgaier,[c] Markus Mezger,[b] Dieter Richter[c] and George Floudas*[a]

Received 16th July 2016,
Accepted 6th September 2016

DOI: 10.1039/c6sm01622g

www.rsc.org/softmatter

The absence of entanglements, the more compact structure and the faster diffusion in melts of cyclic poly(ethylene oxide) (PEO) chains have consequences on their crystallization behavior at the lamellar and spherulitic length scales. Rings with molecular weight below the entanglement molecular weight ($M < M_e$), attain the equilibrium configuration composed from twice-folded chains with a lamellar periodicity that is half of the corresponding linear chains. Rings with $M > M_e$ undergo distinct step-like conformational changes to a crystalline lamellar with the equilibrium configuration. Rings melt from this configuration in the absence of crystal thickening in sharp contrast to linear chains. In general, rings more easily attain their extended equilibrium configuration due to strained segments and the absence of entanglements. In addition, rings have a higher equilibrium melting temperature. At the level of the spherulitic superstructure, growth rates are much faster for rings reflecting the faster diffusion and more compact structure. With respect to the segmental dynamics in their semi-crystalline state, ring PEOs with a steepness index of ~34 form some of the "strongest" glasses.

1. Introduction

Polymer topology matters with respect to the structure, packing and dynamics of chains. This relation can best be explored with ring or cyclic polymers.[1] Ring polymers have a unique topology that is lacking free ends. This peculiarity of rings fascinated scientists for several decades as the major chain relaxation found in linear polymers (reptation) is completely suppressed. Interestingly, nature employs ring topologies, for example, in packing chromatin rings in nucleosomes providing easy access to genetic information.[2–4]

For entropic reasons ring polymers are not interpenetrating and rather contract into a folded form of a branched "lattice animal". Hence, the more compact conformations with an asymptotic conformation of a crumpled globule for larger chains.[5] Furthermore, the exponent, ν, in the mean-square radius of gyration, $\langle R_g^2 \rangle \sim N^{2\nu}$ is $\nu \sim 2/5$ to $\nu \sim 1/3$ with increasing molecular weight, as suggested by theory[5] and supported by simulation.[6–8] Ring polymers diffuse faster than linear polymers (with $D \sim N^{2.3\pm0.1}$, for large N similar to linear chains but with a pre-factor that is larger for rings). Rings relax the stress much faster than linear chains and the zero-shear viscosity scales as $\eta \sim N^{1.4\pm0.2}$, *i.e.*, with a much weaker dependence than the $N^{3.4}$ scaling for entangled linear chains.[8,9] These distinct structural features of the ring topology are expected to have some dynamic consequences. A first test of the dynamics was recently made in a series of ring poly(ethylene oxide)s (PEO) by small-angle neutron scattering and neutron spin-echo (NSE) spectroscopy.[10–13] It revealed fast Rouse relaxation of loops relaxing like short unentangled chains and slower loop motion with a lattice animal-like loop displacement.

Since the ring topology affects the polymer coil conformations (*i.e.*, with more compact conformations), as well as the diffusion, zero-shear viscosity and Rouse dynamics, it is likely that it will leave a fingerprint on the nucleation and overall crystallization behavior. After all, the crystalline structure is nucleated and grown from the melt state and to the extent that the melt conformations and dynamics of ring and linear chains differ their semicrystalline state should also be different. In this respect, several studies explored the effect of chain topology on ring crystallization, however, with conflicting results. These were recently reviewed extensively in ref. 14. For example, single crystals of ring poly(ε-caprolactone) (PCL)[15] and of poly(tetrahydrofuran) (PTHF)[16] were prepared from solution and studied by AFM.

[a] *Department of Physics, University of Ioannina, P.O. Box 1186, 451 10 Ioannina, Greece. E-mail: gfloudas@uoi.gr*
[b] *Institute of Physics, Johannes Gutenberg University Mainz and Max Planck Institute for Polymer Research, 55128 Mainz, Germany*
[c] *Jülich Centre for Neutron Science and Institute for Complex Systems, Forschungszentrum Jülich GmbH, 52425 Jülich, Germany*

† Electronic supplementary information (ESI) available: DSC, small-angle X-ray scattering and DS results. See DOI: 10.1039/c6sm01622g

With respect to the lamellar thickness and long period conflicting reports were presented for PCL[14,16] and poly(L-lactide) (PLLA).[17] The nucleation and spherulitic growth was reported for polyethylene (PE),[18] PCL[19–23] and PTHF[24,25] ring polymers. Although there is consensus on the higher nucleation density for ring polymers, the structure of spherulites (banded in PHTF *vs.* classical in PCL) and spherulitic growth rate (slower in PTHF, PE and faster in PCL, with respect to their linear analogues) remains an open question. Lastly, conflicting reports exist also for the crystallization/melting temperatures of ring polymers and in some cases for the overall degree of crystallinity. As an example, lower melting temperatures were reported for PTHF,[24,25] PE,[18] PLA,[26] PEO[27,28] and PCL[29] while other studies reported a higher melting temperature for polymeric alkanes,[30] PE[31] and PCL.[15,16,20,32] In the latter studies[15,16,20] the higher melting temperature for rings ($T_f^\infty = \Delta H^\circ/\Delta S^\circ$, where T_f^∞ is the equilibrium melting temperature, and ΔH°, ΔS°, the changes in the enthalpy and entropy at the transition point) was attributed to the lower configurational entropy in the melt state of the more compact ring topologies as opposed to linear chains.

Here we employ the same ring PEOs investigated earlier with respect to the structure and dynamics in the melt state with NSE.[10–13] We investigate their crystallization behavior by DSC, and their crystal structure at the levels of unit cell, crystalline lamellar and spherulitic superstructure, respectively, by wide-angle X-ray scattering, small-angle X-ray scattering and polarizing optical microscopy (POM). Lastly, the segmental dynamics of the semi-crystalline polymers are investigated with dielectric spectroscopy. All experiments refer to rather low molecular weight polymers for which the most extended configurations can be attained. With these tools we address the following open questions: (a) how different is the structure at the different length scales as well as the thermodynamics under equilibrium and non-equilibrium conditions and (b) how the segmental dynamics within the amorphous phase of the semi-crystalline samples differ between ring and linear topologies. We find that thermal annealing plays a crucial role in reaching the equilibrium twice folded configuration of ring polymers. Ring polymers undergo a distinct step-like conformational change from a crystalline lamellar composed of strained segments within the amorphous domains to a crystalline lamellar with the equilibrium configuration. Rings melt from this configuration in the absence of crystal thickening. In general, rings more easily attain their extended equilibrium configuration due to strained segments and the absence of entanglements. In addition, there is a higher equilibrium melting temperature for rings.

2. Experimental section

(a) Materials

Cyclic PEOs were obtained from the linear polyethylene glycols as described elsewhere. Linear polymers synthesized *via* anionic polymerization were used as precursors for the ring-closure reaction. Multiple fractionation minimized the linear contamination of the cyclic polymers. The number average molecular weights of the linear polymers were obtained by end-group analysis using ^{1}H-NMR in pyridine-d_5 as solvent and by size exclusion chromatography (SEC) using PEO calibration.[13] Both analytical methods are non-applicable for ring shaped PEO. As the cyclisation reaction does not change the molecular weight, identical values were assumed for the linear and the ring versions. Four samples were prepared with the following characteristics: (1) M_n(NMR) = 1860 g mol^{-1}, M_n(SEC) = 1860 g mol^{-1} (L2k, R2k); (2) M_n(NMR) = 5100 g mol^{-1}, M_n(SEC) = 5000 g mol^{-1} (L5k, R5k); (3) M_n(NMR) = 10 100 g mol^{-1}, M_n(SEC) = 9400 g mol^{-1} (L10k, R10k) and (4) M_n(NMR) = 20 100 g mol^{-1}, M_n(SEC) = 18 600 g mol^{-1} (L20k, R20k). The fractions of linear polymer in the ring samples were $\leq$1% for the rings R2k, R5k, and R10k. For R20k 3.7% were measured using the NMR method described above. The sample characteristics are summarized in Table 1. SEC traces of the purified ring polymers are given in Fig. S1, ESI.†

Table 1 Characteristics of the ring polymers and their linear precursors

	Ring polymers		Linear precursors	
Sample code	Linear unimer (%)	M_w/M_n	M_n (kg mol^{-1})	M_w/M_n
2k	0.3	1.02	1.860	1.02
5k	0.4	1.01	5.100	1.01
10k	1.0	1.02	10.100	1.02
20k	3.7	1.03	20.100	1.02

(b) Differential scanning calorimetry

The thermal properties were studied with a Q2000 (TA Instruments) differential scanning calorimeter (DSC). Cooling and heating cycles were performed at a rate of 10 K min^{-1} and in a temperature range between 173 K and 393 K. The instrument was calibrated for best performance on the specific temperature range and heating/cooling rate. The calibration sequence included a baseline calibration for the determination of the time constants and capacitances of the sample and reference sensor using a sapphire standard, an enthalpy and temperature calibration for the correction of thermal resistance using indium as standard (ΔH = 28.71 J g^{-1}, T_m = 428.8 K), and a heat capacity calibration with sapphire standard.

(c) Polarizing optical microscopy

A Zeiss Axioskop 40, equipped with a video camera and a fast frame grabber was used to follow the superstructure formation in the graft and block-graft systems. A Linkam temperature control unit (THMS600), equipped with TMS94 temperature programmer, was employed for the temperature-dependent studies. Images were recorded following slow cooling (1 K min^{-1}) from the melt state. In a second experiment the kinetics of superstructure formation were investigated by performing T-jumps from high temperatures (T = 353 K) to different final crystallization temperatures where the growth of the crystalline complex was followed. Subsequently, the system was heated with 1 K min^{-1} and the apparent melting temperature of the superstructure was recorded.

(d) X-Ray scattering

Small-angle (SAXS) and wide-angle X-ray scattering (WAXS) measurements were made using CuKα radiation (RigakuMicroMax 007 X-ray generator, Osmic Confocal Max-Flux curved multilayer optics). 2D diffraction patterns were recorded on an Mar345 image plate detector at a sample-detector distance of 2240 mm (SAXS) and of 311 mm (WAXS). Intensity distributions as function of the modulus of the total scattering vector, $q = (4\pi/\lambda)\sin(2\theta/2)$, where 2θ is the scattering angle, were obtained by radial averaging of the 2D datasets. Oriented fibers of 1.0 mm diameter were prepared by a mini-extruder at 293 K. In the WAXS experiments, temperature dependent measurements were made in the range from 293 K to 323 K in 5 K steps on heating. SAXS experiments on the crystallization kinetics were made as follows: the sample was first heated to an initial temperature of 353 K followed by fast cooling to different final crystallization temperatures. Sufficient time (typically 1–8 hours) was given at each temperature to allow crystallization. Following this time interval, a 1 h long measurement was made to obtain its crystalline structure. Subsequently, the sample was slowly heated with a constant temperature ramp of 0.15 K min^{-1} to 353 K. During this ramp, 2–3 min long measurements were made to record the crystal thickness as a function of temperature up to the melting point. For example, for the L5k PEO, the following crystallization temperatures were chosen: 321 K, 322 K, 323 K, 324 K and 325 K. For the 5k Ring PEO, the crystallization temperatures were: 321 K, 323 K and 325 K.

(e) Dielectric spectroscopy (DS)

Dielectric spectroscopy measurements were made as a function of temperature in the range from 163 K to 303 K using a Novocontrol Alpha frequency analyzer (frequency range from 10^{-2} to 10^{7} Hz). The complex dielectric permittivity $\varepsilon^* = \varepsilon' - i\varepsilon''$, where ε' is the real and ε'' is the imaginary part, is a function of frequency ω, temperature T, and in general pressure P, $\varepsilon^* = \varepsilon^*(\omega, T, P)$.[33–35] In the analysis of the DS spectra we have used the empirical equation of Havriliak and Negami (HN)[36]

$$\varepsilon_{HN}{}^*(\omega, T) = \varepsilon_\infty(T) + \frac{\Delta\varepsilon(T)}{[1 + (i\omega \cdot \tau_{HN}(T))^m]^n} + \frac{\sigma_0(T)}{i\varepsilon_f\omega} \quad (1)$$

where $\tau_{HN}(T, P)$ is the characteristic relaxation time, $\Delta\varepsilon(T, P) = \varepsilon_0(T, P) - \varepsilon_\infty(T, P)$ is the relaxation strength of the process under investigation, m, n (with limits $0 < m, mn \leq 1$) describe, respectively, the symmetrical and unsymmetrical broadening of the distribution of relaxation times, σ_0 is the dc-conductivity and ε_f is the permittivity of the free space. In the fitting procedure, we have used the ε'' values at every temperature and in some cases the ε' data were also used as a consistency check. From, τ_{HN} the relaxation time at maximum loss, τ_{max}, is obtained analytically following:

$$\tau_{max} = \tau_{HN} \cdot \sin^{-1/m}\left(\frac{\pi m}{2(1+n)}\right) \cdot \sin^{1/m}\left(\frac{\pi mn}{2(1+n)}\right) \quad (2)$$

In the temperature range where two relaxation processes contribute to ε^* there are two ways of representing the data. The first one, followed here, is based in a summation of two HN functions and assumes statistical independence in the frequency domain. The second one, proposed by Williams and Watts is a molecular theory for the dipole moment time-correlation function $C_\mu(t)$ (also known as "Williams ansatz").[37] In addition to the measured ε'' spectra the derivative of ε' ($d\varepsilon'/d\ln\omega \sim -(2/\pi)\varepsilon$) have been used in the analysis of the dynamic behavior.[38]

3. Results and discussion

As will become apparent below a number of features of ring PEOs, like crystal thickness, equilibrium melting temperature and overall crystallinity, are strongly influenced by the thermal history. Therefore, in the following we will discuss states away and closer to equilibrium separately. Evidently, much of the confusion in literature is related to this distinction.

(a) States away from equilibrium

In this first part we discuss the crystallization and melting behavior of rings in relation to their linear counterparts under the condition that the crystallization/melting is followed without any annealing procedure. The DSC traces of all linear and ring PEOs investigated herein, obtained with a cooling/heating rate of 10 K min^{-1} are shown in Fig. S2, ESI.† The results from this study are summarized in Table 2 (for the degree of crystallinity the same heat of fusion was employed for the 100% crystalline PEO, namely 196 J g^{-1}).

The traces display a higher crystallization/melting peak for the linear chains as depicted in Fig. 1. As we will discuss below with respect to the states closer to equilibrium, this conclusion is erroneous as it reflects the non-equilibrium nature of folded chains (also seen in ref. 28). For PCL, on the other hand, both apparent and equilibrium melting temperatures were higher for rings. This may imply slower kinetics in PEO. The structure, at the level of the unit cell and crystalline lamellar, were investigated by WAXS and SAXS, respectively. The WAXS patterns of L2k and R2k are shown in Fig. 2 at ambient temperature.

The scattering pattern for L2k exhibits the (021), (110), (120), (112), (032), (024) and (131) Bragg reflections of the ordinary monoclinic PEO structure[39] with lattice parameters a = 0.81 nm, b = 1.30 nm, c = 1.95 nm and β = 125.4°. The pattern for R2k show a less ordered structure with peaks corresponding to the (120) and (032) reflections of the same monoclinic lattice. Hence, both

Table 2 Thermodynamics (apparent melting temperature, heat of fusion, degree of crystallinity, change of entropy) of linear and ring PEOs under non-equilibrium conditions (rate 10 K min^{-1})

PEG	T_m' (K)	X_c	ΔH (J g^{-1})	ΔS (J g^{-1})
L2k	326	0.89	175	0.53
R2k	321	0.67	132	0.41
L5k	328	0.62	122	0.37
R5k	328	0.58	114	0.35
L10k	336	0.85	167	0.50
R10k	330	0.85	166	0.50
L20k	336	0.64	126	0.38
R20k	330	0.57	112	0.34

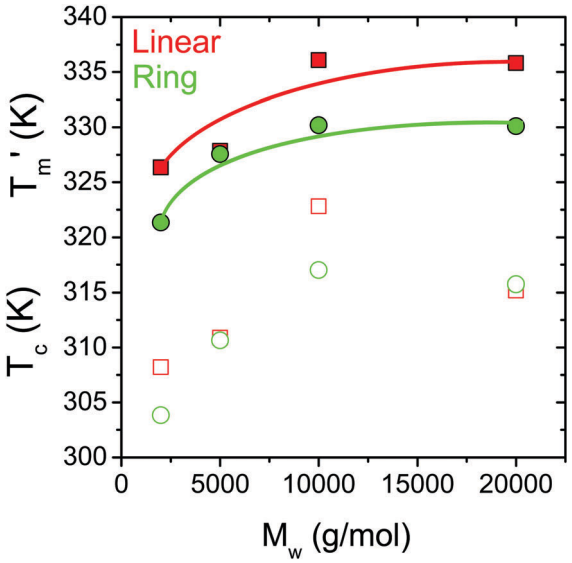

Fig. 1 Crystallization (open symbols) and apparent melting temperature (filled symbols) for linear (red symbols) and ring (green symbols) PEOs. All measurements refer to a heating/cooling rate of 10 K min^{-1}. The lines are a guide for the eye.

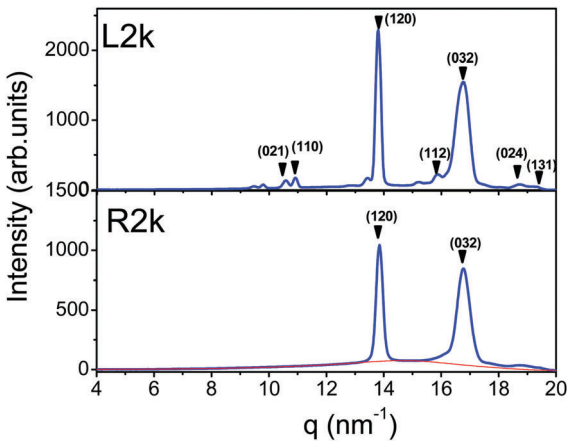

Fig. 2 WAXS patterns of L2k (top) and R2k PEO (bottom). The red line in the latter gives the contribution from the amorphous part. Arrows give the position and (*hkl*) indices of the Bragg reflections corresponding to the monoclinic unit cell of PEO.

linear and ring PEO chains crystallize with an identical unit cell. This shows that at a ~nm length scale the ring topology does not influence the primary crystal structure.

The SAXS curves for some linear and ring PEOs are depicted in Fig. 3 at 298 K, obtained from the extruded fibers without any annealing. The samples, by definition are away from equilibrium. Nevertheless, some interesting features can be seen. For example, for the lowest molecular weight PEOs, (L2k/R2k), the first order diffraction peak of R2k coincides with the second order diffraction peak from L2k. This trend holds approximately for the higher molecular weight samples as well. It can be interpreted as reflecting a more folded structure for rings. We will return to this point in discussing the equilibrium structures.

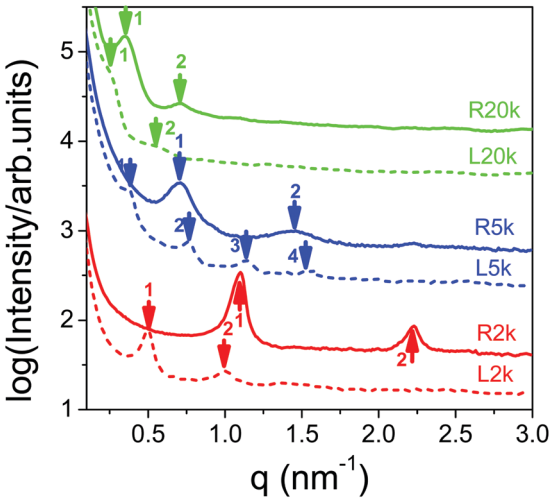

Fig. 3 SAXS patterns for the linear and corresponding ring PEOs under non-equilibrium conditions (*i.e.*, not annealed samples) at 298 K. Arrows with relative peak positions with ratios 1 : 2 : 3 : 4 are shown.

(b) States closer to equilibrium

Here we make the distinction between the lower molecular weight samples (L2k and R2k) that always attain their equilibrium configuration, and the higher molecular weights that in the absence of annealing are away from equilibrium. With an average lamellar thickness of $L = \lambda/(1 + n)$, where λ is the crystalline chain length, $\lambda = M_n/\nu = 12.64$ nm ($\nu = 158.2$ g nm^{-1} is the molar mass per unit length along c axis)[40] and n is the number of folds, L2k has an extended chain conformation (no folds). R2k has also the equilibrium structure with a twice-folded conformation (*i.e.*, the long period for L2k is twice that for the R2k; here with respect to folding of rings we employ the definition used in ref. 27). Hence the chains in both L2k and R2k crystallize with their equilibrium structure. We note here that the entanglement molecular weight for PEO is $M_e \sim 1620$ g mol^{-1}.[41]

For $M > M_e$ a different protocol has to be employed to access the equilibrium conformations. This involves isothermal crystallization from the melt state, followed by slow heating up to the melting point. During the slow heating ramp, the long period is recorded. As an example, we show in Fig. S3 ESI,† the SAXS patterns of L5k, crystallized isothermally at 322 K (from an initial temperature of 353 K) followed by subsequent slow heating. The patterns show the usual lamellar thickening of linear polymers. Fig. 4 depicts similar experiments performed with R5k crystallized isothermally at two different temperatures: 321 K and at 325 K, followed by slow heating to the melting point.

Crystallization of the same sample at the intermediate temperature of 323 K is shown in Fig. S4 (ESI†). The isothermally crystallized R5k displays significantly different behavior than L5k (Fig. 4). Following isothermal crystallization at 321 K the SAXS pattern displays a peak at $q \sim 0.65$ nm^{-1}. The peak position persists on subsequent heating to ~325 K. At higher temperatures a step-like change to $q \sim 0.3$ nm^{-1} is observed reflecting doubling of lamellar periodicity. R5k melts directly

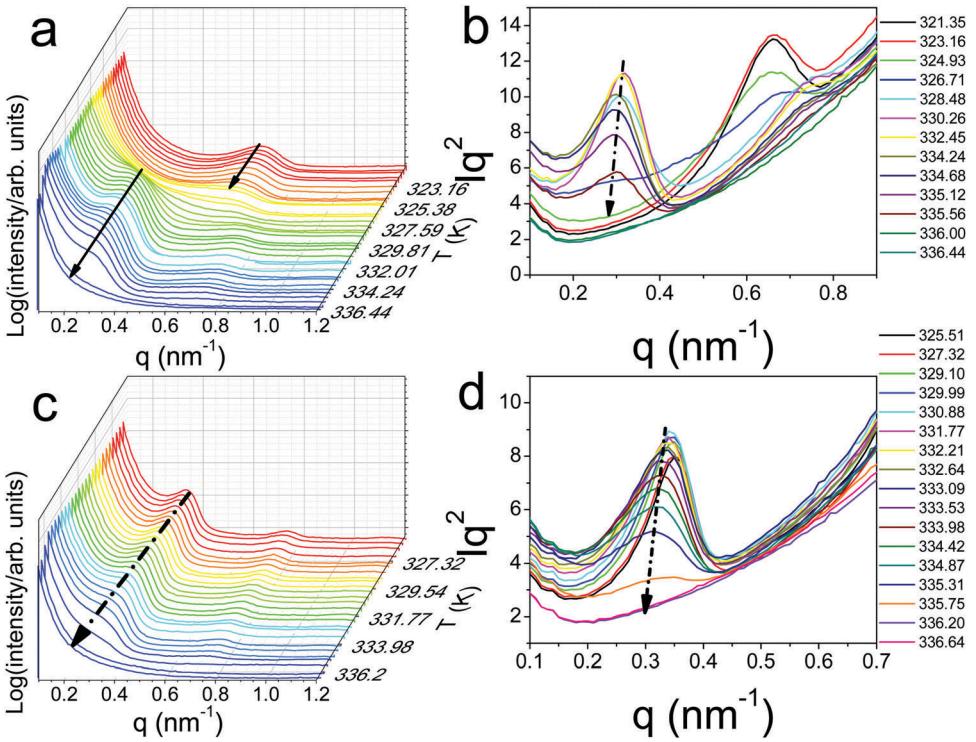

Fig. 4 SAXS patterns of R5k PEO obtained on heating following isothermal crystallization (a) at 321 K and (c) at 325 K. The corresponding Lorentz-normalized patterns are shown in (b) and (d) (the corresponding temperatures are indicated in the inset). Arrows indicate the change in peak position with temperature.

from this state without any further thickening. The isothermal crystallization at 323 K (Fig. S4, ESI†) displays a similar behavior but now the step-like increase takes place at 327 K. More interesting is the behavior of the isothermally crystallized R5k at 325 K (Fig. 4). At this temperature the peak appears already at $q \sim 0.3$ nm^{-1} and the crystalline lamellar is melted directly from this periodicity without any further thickening. We emphasize here the difference between L5k and R5k chains, with the continuous lamellar thickening as opposed to a step-like increase in lamellar periodicity, respectively. More detailed structural information can be obtained from a correlation function analysis of the intensity distributions. The electron density correlation function, $K(z)$, obtained from the inverse Fourier transformation of the intensity distribution, $I(q)$, allows obtaining the long spacing, d, and interlamellar amorphous layer measured along the lamellar normal (d_a). The crystalline lamellar thickness is then obtained as $d_c = d - d_a$. This type of analysis was made for R5k crystallized at the higher temperature (*i.e.* at 325 K) and the result is shown in Fig. S5 (ESI†). From the long spacing, d ($\sim$20 nm), and interlamellar amorphous layer thickness, d_a ($\sim$8 nm) the obtained crystalline lamellar thickness (d_c = 12 nm) is approximately half the corresponding distance of the extended chain conformation for linear chains.

Results on the relation between crystallization temperature and crystal thickness, d_c, from the isothermally crystallized PEOs are summarized in Fig. 5. For the linear PEOs, the data indicate a continuous lamellar thickening process on heating. Following Strobl *et al.*,[42] lines corresponding to the crystallization and re-crystallization temperatures are shown. They both have a general dependence according to the Gibbs-Thomson (GT) equation:

$$T(d_c) = T_f^{\infty} - \frac{2\sigma_e T_f^{\infty}}{\Delta H_f}\frac{1}{d_c} \quad (3)$$

Eqn (3) describes the suppression of the melting temperature of a crystal with thickness, d_c, to temperatures below the equilibrium melting, T_f^{∞}, caused by the excess free energy, σ_e, of the fold surface (ΔH_f is the heat of fusion). The crystallization line, describing the relation between the crystal thickness and the initial crystallization temperature – where the samples were isothermally crystallized – follows as

$$\frac{1}{d_c} = C_c\left(T_c^{\infty} - T\right) \quad (4)$$

where T_c^{∞}, is a controlling temperature. The re-crystallization line depicts the relation of crystal thickness to the temperature range where a continuous lamellar thickening (*i.e.*, re-crystallization) takes place according to:

$$\frac{1}{d_c} = C_R\left(T_c^{\infty} - T\right) \quad (5)$$

This situation for the ring polymers is very different. First, as indicated in Fig. 5, the crystallization line for the ring polymers coincides with the re-crystallization line for linear PEOs. Secondly, and more important, rings undergo distinct conformational changes towards the equilibrium lamellar. When crystallized at

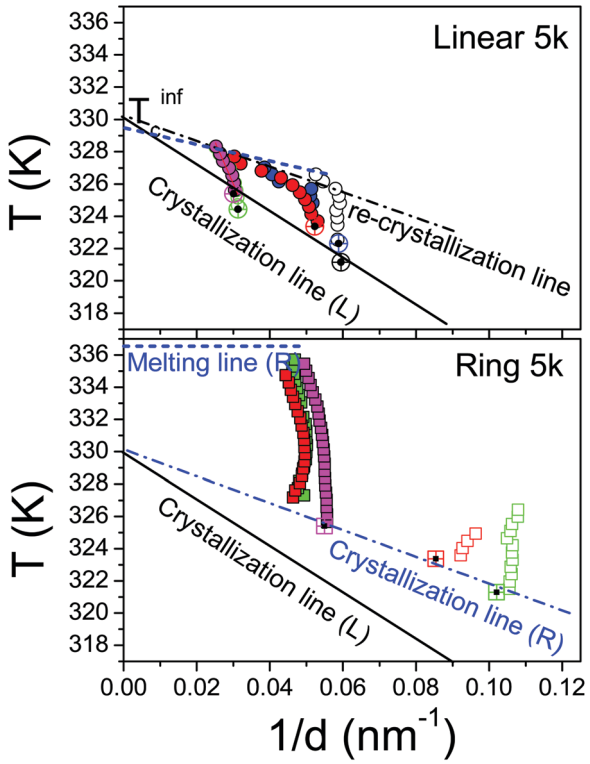

Fig. 5 Results from temperature-dependent SAXS experiments on L5k (top) and R5k (bottom) PEO on the relation between crystallization temperature and long period. The symbols correspond to: (top) (black circles): 321 K, (blue circles): 322 K, (red circles): 323 K, (green circles): 324 K and (magenta circles): 325 K; (bottom): (green squares): 321 K, (red squares): 323 K and (magenta squares): 325 K. For the linear PEO, the crystallization line and re-crystallization lines are shown with solid and dash-dotted lines, respectively, whereas the melting line is shown with a blue dashed line. These lines give the dependence of the crystallization and re-crystallization temperatures on the inverse periodicity. For the ring PEO the crystallization lines is shown with a blue dash-dotted line and the melting line with a blue dashed line. Notice, the higher melting points for the rings (blue dashed line) and that the crystallization line of the ring PEO coincides with the re-crystallization line of the linear PEO.

low temperatures, they undergo a distinct lamellar thickening by doubling of the long period and melt from this configuration without any substantial crystal thickening. When crystallized at higher temperatures (*i.e.*, at 325 K) they immediately attain the equilibrium configuration and melt from this state without any crystal thickening. The equilibrium melting temperature, T_m°, for R5k is at ~337 K (shown with the horizontal dashed line in Fig. 5) whereas for L5k is at ~329 K. Similarly for R10k, the equilibrium melting temperature is at ~336 K, whereas for L10k is at 334 K. In general, rings have a higher melting temperature than linear chains. This was also the conclusion from an earlier investigation on ring PEOs[27] although the precise mechanism was not tracked. This situation for the annealed samples is very different than the ones obtained away from equilibrium (*i.e.*, in Fig. 1 and Table 1). We attribute the confusion in literature with respect to the melting temperature and long period to the different annealing conditions employed for the different samples.

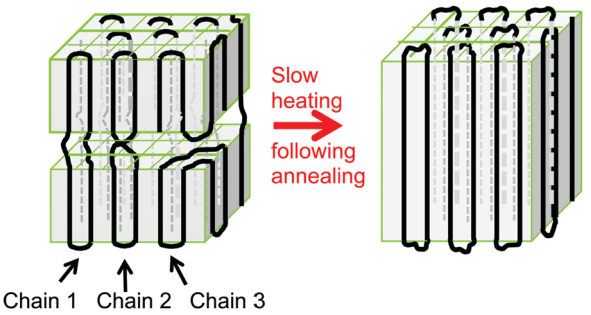

Fig. 6 Three chain configurations in a ring polymer (left) as compared to the final equilibrium structure (right) composed from chains in a twice folded chain conformation.

A question here arises on the reasons for these distinct differences in the long period of rings *vs.* linear chains as seen on slow heating. We address this question with the help of Fig. 6 showing the configurations of three chains in a highly schematic way. Chain 1 has an extended configuration with a twice folded chain. The amorphous part is comprised by segments already in a pre-strained extended configuration. Chain 2 has also a twice folded pattern but it contains a topological constraint within the amorphous part. Chain 3 has a folded configuration within the same crystalline stem. From the three configurations only one can easily attain the final equilibrium configuration (in the right). For example, the configuration of Chain 2 requires substantial re-organization within the crystalline lamellar stems. In addition, its entangled topology within the amorphous domains is not supported by the melt characteristics.[5–9] Chain 3 can only attain the equilibrium conformation by a slow sluggish motion that would inevitably result to continuous lamellar thickening, against the experimental observations. In contrast, Chain 1, with the pre-formed extended chain conformation more easily can attain the equilibrium lamellar. To account for the density within the amorphous domains a small fraction of Chain 3 type conformations in a majority of Chain 1 conformations can be envisaged. The role of the latter is not only to adjust the density but also to fix the position of the amorphous part right in the center of Chain 1. Hence, a distinct feature of the crystalline lamellar in ring polymers is that it is composed from chains that are more extended in the absence of any topological constraints (entanglements). These features more easily allow for the doubling of lamellar periodicity at lower temperatures or to a crystalline lamellar with the equilibrium domain spacing at higher temperatures. Linear polymers, on the other hand, contain topological constraints in their amorphous part. In this case, the only root towards the equilibrium extended conformation is by a slow lamellar thickening process as observed experimentally (Fig. S3, ESI†).

At this point we recall a single report on lamellar doubling in linear ultra-high molecular weight polyethylene crystallized from solution.[43] This finding was discussed in terms of mutual chain rearrangement between adjacent lamellae involving a sliding motion along the axis resulting to the doubling of

lamellar thickness. Such type of sliding motions may also be held responsible for some peculiar features seen in the SAXS data of rings. Heating the sample at a rate of 0.15 K min^{-1} causes at *ca.* 326.71 K (Fig. 4b) almost the complete disappearance of the scattering peaks, suggesting either (i) that almost all crystalline regions were molten before the better ordered and thicker crystalline state was formed at higher temperature (and later times), or (ii) changing contrast between amorphous and crystalline domains by the slow sliding motions of chains. Another peculiar feature of the long period shown in Fig. 5 is the fact that upon increasing temperature, the long period is first becoming smaller before it slightly increases. This feature may also reflect slow chain sliding motions resulting in annihilation of defects. Lastly, we should comment on the proposed thickening mechanism for PCL rings. The proposed thickening mechanism was by a continuous sliding motion of type 3 chains. In contrast, our results for PEO rings suggest a distinct lamellar thickening process by doubling of the long period. This favors chain configurations of type 1 (with the extended configuration).

We also need to comment on the higher melting temperature for rings. We mention here that earlier work[14,15] discussed the different melting temperatures of linear and ring polymers by a modified GT equation. The melting temperature is defined as $T_f^{\infty} = (H_{melt} - H_{cr})/(S_{melt} - S_{cr})$, where the indices refer to the melt and crystalline states, respectively. Based on the more compact structures of rings in the their melt state the expectation is that $S_{melt}(R) < S_{melt}(L)$. In addition, given the more stretched segmental conformations within the amorphous domains (Chain 1) the expectation is that the same inequality will hold for the crystalline state as well, *i.e.*, $S_{cr}(R) < S_{cr}(L)$. Hence the higher equilibrium melting temperature of rings reflects a delicate balance of the configurational entropies of the melt and crystal states of ring and linear chains so that: $S_{melt}(R) - S_{cr}(R) < S_{melt}(L) - S_{cr}(L)$.

Superstructure formation. The POM images for both linear and ring polymers display the usual Maltese cross extinction pattern shown in Fig. 7. However, some features for rings are distinct. For R2k, the superstructure is spherulitic at 312 K but is truncated when crystallized at 317 K. We have analyzed the (linear) growth rates of linear and ring PEOs using the crystallization theory of Lauritzen and Hoffman[44] (crystal growth by secondary nucleation) which has a molecular basis, in that, it accounts for the diffusion and crystallization of chains. The crystal growth rate is given by

$$G = G_0 \exp\left(-\frac{B}{T - T_0}\right) \exp\left(-\frac{K_g(i)}{T\left(T_f^{\infty} - T\right)}\right) \qquad (6)$$

where G_0 is the growth rate constant, B is the activation parameter for transport of crystallizing units across the crystal-liquid interface, T_0 is the "ideal" glass temperature located below T_g, and $K_g(i)$ is the nucleation rate constant that contains information on the lateral- and fold-surface free energies and the heat of fusion (in the model proposed by Strobl,[42] the equilibrium melting temperature is replaced by the zero-growth

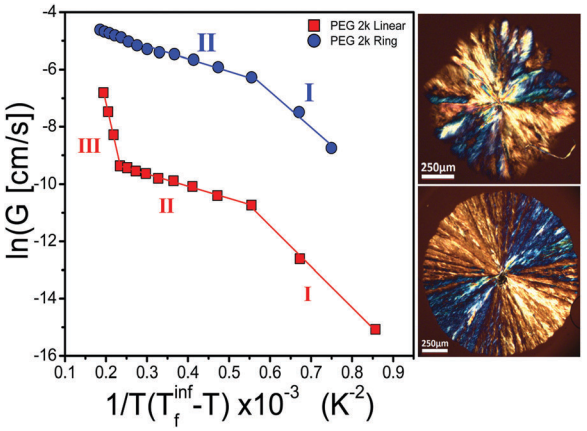

Fig. 7 (left) Growth rates of superstructures as a function of scaled temperature with respect to the equilibrium melting point, T_f^{∞}, for the L2k (squares) and R2k (circles) PEO. The actual temperature range was 311 to 324 K for L2k and 304 to 318 for R2k. Latin letters I, II and III indicate the three growth regimes. Lines are guides to the eye. (right) Representative POM images of superstructures of R2k at 317 K (top) and at 312 K (bottom). A scale bar of 250 μm is shown in both.

temperature). The symbol i represent a number associated to the particular regime and is equal to 4 for regimes I and III and equal to 2 for regime II. The three regimes differ according to the competition between the rate of deposition of secondary nuclei (d) and the rate of lateral surface spreading (g); in regime I, $d \ll g$ and appears at very low supercoolings, in regime II, $d \approx g$ and occurs for intermediate supercooling and in regime III, $d > g$, and corresponds to very high supercoolings. Taking the natural logarithm of the growth rates and plotting $\ln G(i)$ *vs.* $(T_c\Delta T)^{-1}$ the different regimes can be identified from the distinct changes in slopes. Notice, that the abscissa in Fig. 7 is corrected for the different equilibrium melting temperatures for rings *vs.* linear chains. Thus the three regimes are clearly shown for L2k. We mention here that work by Kovacs *et al.* suggested that the growth kinetics of short chains of PEO is controlled by the folding of chains.[45] In R2k, growth is dominated by regimes I and II. But the most pertinent feature of rings is that the growth rates are some orders of magnitude higher than for its linear counterpart. Note that a faster growth rate for ring PEOs was also found in another study albeit at a single temperature.[28] This feature for the ring polymers is anticipated by the faster diffusion in the melt state associated with the lower melt viscosity and more compact structure of rings.[5–13] From the LH analysis[44] of the spherulitic growth rates the following parameters were extracted for L2k; $K_g(I) = 22\,300$ K^2, $K_g(II) = 7600$ K^2, $K_g(III) = 78\,500$ K^2 as compared to R2k; $K_g(I) = 20\,500$ K^2, $K_g(II) = 9400$ K^2. The corresponding product of the lateral surface free energy, σ, with the fold surface free energy, σ_e, is $\sigma\sigma_e(I) \sim 120$ erg^2 cm^{-4}, $\sigma\sigma_e(II) \sim 80$ erg^2 cm^{-4}, $\sigma\sigma_e(III) \sim 420$ erg^2 cm^{-4} for L2k and $\sigma\sigma_e(I) \sim 110$ erg^2 cm^{-4}, $\sigma\sigma_e(II) \sim 100$ erg^2 cm^{-4} for R2k (the calculation was based on: width of a chain of $b = 4.62$ Å, $\Delta H_f = 2.36 \times 10^9$ erg cm^{-2} and the VFT parameters reported below).

Local segmental dynamics. The local segmental dynamics of PEO within the amorphous phase of the semicrystalline

chains have been studied by DS. The question here is how the segmental mobility of ring polymers differ from their linear counterparts. The absence of chain ends and the doubly folded chains back to the crystal in the ring case (*i.e.*, Chain 1, Fig. 6) could impose more constraints on the segmental motion. On the other hand, the degree of crystallinity plays also an important role as lower crystallinity implies longer loops away from the crystal and hence less restricted segments that could result to faster segmental dynamics. Hence, the segmental dynamics will be influenced by both (a) the tethering of chains at the crystal phase and (b) the length of excursion of folded chains. The results for the segmental dynamics are discussed with respect to the Arrhenius representation of characteristic times. The latter were extracted by fitting the dielectric loss curves (Fig. S6 and S7, ESI†) in Fig. 8. Linear PEO of high molecular weight (M_w = 32 500 g mol^{-1})[46] exhibits a local segmental process that conforms to the Vogel–Fulcher–Tammann (VFT) equation:

$$\tau = \tau_0 \exp\left(\frac{B}{T - T_0}\right) \quad (7)$$

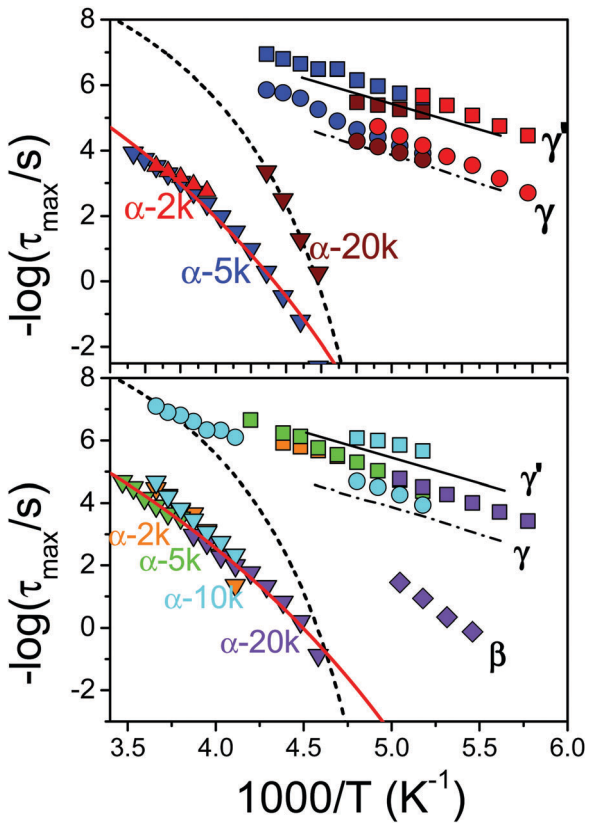

Fig. 8 Arrhenius relaxation map for the segmental (α-) (triangles) and for the more local γ (circles) and γ′ (squares) processes in linear (top) and ring (bottom) PEOs. The symbols correspond to: (top) (red): 2k, (blue): 5k and (wine): 20k; (bottom) (orange): 2k, (green): 5k, (cyan): 10k and (magenta): 20k. Dashed, dashed-dotted and solid black lines give the segmental, local γ and γ′ processes of linear PEO of high molecular weight. The red-lines are fits to the VFT equation for the segmental processes in the lower molecular weights of linear and for all molecular weights for the ring PEOs.

where τ_0 (=10^{-12} s) is the relaxation time in the limit of very high temperatures, B = 1010 K is the activation parameter and T_0 = 182 K is the "ideal" glass temperature.

Notice that this term is identical to the "diffusion" term in eqn (6) for the superstructure growth. Linear L20k follows the same VFT dependence but the lower molecular weights follow a less steep dependence with $\tau_0 = 10^{-12}$ s, B = 2550 ± 50 K and T_0 = 140 ± 3 K (T_g = 219 K). At lower temperatures all linear polymers are characterized by two local relaxation termed γ and γ′ with an Arrhenius T-dependence and activation energies of 32 and 25 kJ mol^{-1}, respectively.[46] Ring PEOs in their glassy state exhibit the same (γ and γ′) local processes. This further confirms the local nature of these glassy modes as are unaffected by the ring topology. In addition to these processes another slower process exists in the glassy state, indicated as β-process, that is more evident in R20k. This process has been discussed in terms of PEO segments confined within the restricted amorphous phase of PEO.[47] On the other hand, the segmental dynamics in the rings are independent of molecular weight and can be described by a single VFT process with parameters: $\tau_0 = 10^{-12}$ s (held fixed), B = 2800 ± 100 K and T_0 = 120 ± 3 K (T_g = 207 K). In comparing the segmental dynamics of linear and ring PEOs, it appears that the latter, are more "strong" glasses, as reflected in the lower value of the steepness index, m^*, defined as[48]

$$m^* = \frac{\partial(\log \tau)}{\partial\left(\frac{T_g}{T}\right)_{T=T_g}} \quad (8)$$

which is equivalent to the slope in the "fragility" plot of log τ *vs.* T_g/T. The steepness index can readily be calculated from

$$m^* = \frac{BT_g}{(T_g - T_0)^2(\ln 10)} \quad (9)$$

and amount to ~40 ± 1 and 34 ± 2 for the linear (L2k, L5k) and ring PEOs, respectively. This value of the steepness index is characteristic of "strong" glass formers and shows a dependence on the ring structure. Actually with a steepness index of ~34, ring PEOs form one of the "strongest" glasses.[49] This low value for rings is in agreement with the notion of more extended chains within the amorphous domains (Chain 1 in Fig. 6). We mention here that an earlier study[28] on quenched ring PEOs of low molecular weights indicated somewhat higher T_g's for the ring polymers.

4. Conclusion

The absence of entanglements, the more compact structure and the faster chain diffusion in melts of ring PEOs have immediate consequences on their crystallization behavior. Ring topology has little effect on the structure at the ~nm length scale but it strongly affects the structure at intermediate (lamellar) and global (spherulite) length scales as well as the dynamics. The main conclusions from the present study can be summarized as follows:

• With respect to the unit cell, both rings and linear chains upon crystallization adopt the same unit cell (7/2 helix; monoclinic unit cell) with identical lattice parameters.

• At the level of the lamellar structure the data revealed a strong effect of molecular weight and annealing. Rings below 2k attain only one configuration, *i.e.*, the equilibrium one, composed from twice-folded chains with a lamellar periodicity that is half of the corresponding linear chains. Rings above 2k undergo distinct step-like conformational changes from a crystalline lamellar with strained segments within the amorphous domains to a crystalline lamellar with the equilibrium configuration (composed from twice-folded chains). Rings melt from this configuration in the absence of crystal thickening in sharp contrast to linear chains. In general, rings more easily attain their extended equilibrium configuration due to strained segments and absence of entanglements. In addition, there is a higher equilibrium melting temperature for rings.

• At the level of the spherulitic superstructure, growth rates are much faster for rings reflecting the – theoretically predicted – faster diffusion and more compact structure in the melt state of rings *vs.* linear chains.

• Lastly, with respect to the segmental dynamics, a steeper dependence of the characteristic relaxation times on temperature is obtained for rings reflecting the strained segments in the amorphous domains.

The findings with respect to unit cell and the spherulitic superstructure are not new for rings. However, the finding on the melting mechanism for rings with a distinct doubling of the long period has not been reported in earlier studies on ring polymers. It is a unique mechanism resulting from the absence of topological constraints (entanglements) for ring polymers. In addition, the effect of topology on the segmental dynamics is examined here for the first time.

Acknowledgements

This work was co-financed by the E. U.- European Social Fund and the Greek Ministry of Development – GSRT in the framework of the THALIS program, and the ''Excellence in the Research Institutes'' program. The current work was also supported by the Research unit on Dynamics and Thermodynamics of the UoI co-financed by the European Union and the Greek state under NSRF 2007–2013 (Region of Epirus, call 18). J. M. and M. M. acknowledge the MAINZ Graduate School of Excellence, funded through the Excellence Initiative (DFG/GSC 266). We thank Dr Dimitris Vlassopoulos (FORTH) for discussions concerning the rheology of ring polymers.

Notes and references

1 T. McLeish, Floored by the Rings, *Nat. Mater.*, 2008, **7**, 933–935.
2 S. Backert, B. L. Nilesen and T. Börner, The Mystery of the Rings: Structure and Replication of Mitochondrial Genomes from Higher Plants, *Trends Plant Sci.*, 1997, **2**, 477–483.
3 T. Cremer and C. Cremer, Chromosome Territories, Nuclear Architecture and Gene Regulation in Mammalian Cells, *Nat. Rev. Genet.*, 2001, **2**, 292–301.
4 A. Rosa and R. Everaers, Structure and Dynamics of Interphase Chromosomes, *PLoS Comput. Biol.*, 2008, **4**, 1–10.
5 A. Y. Grosberg, S. K. Nechaev and E. I. Shakhnovich, The Role of Topological Constraints in the Kinetics of Collapse of Macromolecules, *J. Phys.*, 1988, **49**, 2095–2100.
6 J. D. Halverson, G. S. Grest, A. Y. Grosberg and K. Kremer, Rheology of Ring Polymer Melts: From Linear Contaminants to Ring-Linear Blends, *Phys. Rev. Lett.*, 2012, **108**, 038301.
7 J. D. Halverson, W. B. Lee, G. S. Grest, A. Y. Grosberg and K. Kremer, Molecular Dynamics Simulation Study of Nonconcatenated Ring Polymers in a Melt. I. Statics, *J. Chem. Phys.*, 2011, **134**, 204904.
8 J. D. Halverson, W. B. Lee, G. S. Grest, A. Y. Grosberg and K. Kremer, Molecular Dynamics Simulation Study of Nonconcatenated Ring Polymers in a Melt. II. Dynamics, *J. Chem. Phys.*, 2011, **134**, 204905.
9 M. Kapnistos, M. Lang, D. Vlassopoulos, W. Pyckhout-Hintzen, D. Richter, D. Cho, T. Chang and M. Rubinstein, Unexpected Power-law Stress Relaxation of Entangled Ring Polymers, *Nat. Mater.*, 2008, **7**, 997–1002.
10 D. Richter, S. Gooßen and A. Wischnewski, Celebrating Soft Matter's 10th Anniversary: Topology matters: Structure and Dynamics of Ring Polymers, *Soft Matter*, 2015, **11**, 8535–8549.
11 S. Gooßen, M. Krutyeva, M. Sharp, A. Feoktystov, J. Allgaier, W. Pyckhout-Hintzen, A. Wischnewski and D. Richter, Sensing Polymer Chain Dynamics through Ring Topology: A Neutron Spin Echo Study, *Phys. Rev. Lett.*, 2015, **115**, 148302.
12 S. Gooßen, A. R. Brás, M. Krutyeva, M. Sharp, P. Falus, A. Feoktystov, U. Gasser, W. Pyckhout-Hintzen, A. Wischnewski and D. Richter, Molecular Scale Dynamics of Large Ring Polymers, *Phys. Rev. Lett.*, 2014, **113**, 168302.
13 A. R. Brás, R. Pasquino, T. Koukoulas, G. Tsolou, O. Holderer, A. Radulescu, J. Allgaier, V. G. Mavrantzas, W. Pyckhout-Hintzen, A. Wischnewski, D. Vlassopoulos and D. Richter, Structure and Dynamics of Polymer Rings by Neutron Scattering: Breakdown of the Rouse Model, *Soft Matter*, 2011, **7**, 11169–11176.
14 R. A. Pérez-Camargo, A. Mugica, M. Zubitur and A. J. Müller, Crystallization of Cyclic Polymers, *Adv. Polym. Sci.*, 2015, DOI: 101007/12_2015_326.
15 H.-H. Su, H.-L. Chen, A. Díaz, M. T. Casas, J. Puiggalí, J. N. Hoskins, S. M. Grayson, R. A. Pérez and A. J. Müller, New Insights on the Crystallization and Melting of Cyclic PCL Chains on the Basis of a Modified Thomson-Gibbs Equation, *Polymer*, 2013, **54**, 846–859.
16 E. J. Shin, W. Jeong, H. A. Brown, B. J. Koo, J. L. Hedrick and R. M. Waymouth, Crystallization of Cyclic Polymers: Synthesis and Crystallization Behavior of High Molecular Weight Cyclic Poly(ε-caprolactone)s, *Macromolecules*, 2011, **44**, 2773–2779.

17 H. Tsuji, Poly(lactide) Stereocomplexes: Formation, Structure, Properties, Degradation and Applications, *Macromol. Biosci.*, 2005, **5**, 569–597.
18 T. Kitahara, S. Yamazaki and K. Kimura, Effects of Topological Constraint and Knot Entanglement on the Crystals Growth of Polymers Proved by Growth Rate of Spherulite of Cyclic Polyethylene, *Kobunshi Ronbunshu*, 2011, **68**, 694–701.
19 J. Wang, Z. Li, R. A. Pérez, A. J. Müller, B. Zhang, S. M. Grayson and W. Hu, Comparing Crystallization Rates between Linear and Cyclic Poly(epsilon-caprolactones) *via* Fast-scan Chip-calorimeter Measurements, *Polymer*, 2015, **63**, 34–40.
20 M. E. Córdova, A. T. Lorentzo, A. J. Müller, J. N. Hoskins and S. M. Grayson, A Comparative Study on the Crystallization Behavior of Analogous Linear and Cyclic Poly(ε-caprolactones), *Macromolecules*, 2011, **44**, 1742–1746.
21 R. A. Pérez, M. E. Córdova, J. V. López, J. N. Hoskins, B. Zhang, S. M. Grayson and A. J. Müller, ''Nucleation, crystallization, self-nucleation and thermal fractionation of cyclic and linear poly(e-caprolactone)s'', *React. Funct. Polym.*, 2014, **80**, 71–82.
22 Z. Li, J. Wang, R. A. Pérez-Camargo, A. J. Müller, B. Zhang, S. M. Grayson and W. Hu, Non-monotonic molecular weight dependence of crystallization rates of linear and cyclic poly(epsilon-caprolactone)s in a wide temperature range, *Polym. Int.*, 2016, **65**, 1074–1079.
23 J. V. López, R. A. Pérez-Camargo, B. Zhang, S. M. Grayson and A. J. Müller, ''The Influence of Small Amounts of Linear Polycaprolactone Chains on the Crystallization of Cyclic Analogue Molecules'', *RSC Adv.*, 2016, **6**, 48049–48063.
24 H. Takeshita, M. Poovarodom, K. Kiya, F. Arai, K. Takenaka, M. Miya and T. Shiomi, Crystallization Behavior and Chain Folding Manner of Cyclic, Star and Linear Poly(tetrahydrofuran)s, *Polymer*, 2012, **53**, 5375–5384.
25 Y. Tezuka, T. Ohtsuka, K. Adachi, R. Komiya, N. Ohno and N. Okui, Defect-free Ring Polymers: Size Controlled Cyclic Poly(tetrahydrofuran) Consisting Exclusively of the Monomer Unit, *Macromol. Rapid Commun.*, 2008, **29**, 1237–1241.
26 N. Sugai, S. Asai, Y. Tezuka and T. Yamamoto, Photoinduced Topological Transformation of Cyclized Polylactides for Switching the Properties of Homocrystals and Stereocomplexes, *Polym. Chem.*, 2015, **6**, 3591–3600.
27 G. E. Yu, T. Sun, Z. G. Yan, C. Price, C. Booth, J. Cook, A. J. Ryan and K. Viras, Low-molar-mass Cyclic Poly(oxyethylene)s Studied by Raman Spectroscopy, X-ray Scattering and Differential Scanning Calorimetry, *Polymer*, 1997, **38**, 35–42.
28 S. Nam, *Dynamics of Cyclic and Linear Poly(oxyethylene), and Threading Conformation in their Blends*, PhD Dissertation, Georgia Institute of Technology, 2006.
29 H. Li, R. Jérome and P. Lecomte, Synthesis of Tadpole-shaped Copolyesters based on Living Macrocyclic Poly(ε-caprolactones), *Polymer*, 2006, **47**, 8406–8413.
30 K.-S. Lee and G. Wegner, Linear and Cyclic Alkanes (C_nH_{2n+2}, C_nH_{2n})$n > 100$. Synthesis and Evidence for Chain-Folding, *Makromol. Chem., Rapid Commun.*, 1985, **6**, 203–208.
31 C. W. Bielawski, D. Benitez and R. H. Grubbs, An ''Endless'' Route to Cyclic Polymers, *Science*, 2002, **297**, 2041–2044.
32 K. Schäler, E. Ostas, K. Schröter, T. Thurn-Albrecht, W. H. Binder and K. Saalwächter, Influence of Chain Topology on Polymer Dynamics and Crystallization. Investigation of Linear and Cyclic Poly(ε-caprolactone)s by ^{1}H Solid-state NMR Methods, *Macromolecules*, 2011, **44**, 2743–2754.
33 F. Kremer and A. Schoenhals, *Broadband Dielectric Spectroscopy*, Springer, Berlin, 2002.
34 G. Floudas, in Dielectric Spectroscopy, ed. K. Matyjaszewski and M. Möller, *Polymer Science: A Comprehensive Reference*, Elsevier BV, Amsterdam, 2012, vol. 2.32, pp. 825–845.
35 G. Floudas, M. Paluch, A. Grzybowski and K. L. Ngai, *Molecular Dynamics of Glass-Forming Systems. Effects of Pressure*, Springer, 2011.
36 S. Havriliak and S. A. Negami, A complex plane representation of dielectric and mechanical relaxation processes in some polymers, *Polymer*, 1967, **8**, 161–210.
37 G. Williams and D. C. Watts, in *NMR Basic Principles and Progress*, ed. P. Diehl, E. Flicke and E. Kosfeld, Springer, Berlin, 1971, vol. 4, p. 271.
38 P. A. M. Steeman and J. Turnhout, Fine Structure in the Parameters of Dielectric and Viscoelastic Relaxation, *Macromolecules*, 1994, **27**, 5421–5427.
39 Y. Takahashi and H. Tadokoro, Structural Studies of Polyethers, $(-(CH_2)_m-O-)_n$. X. Crystal Structure of Poly(ethylene oxide), *Macromolecules*, 1973, **6**, 672–675.
40 C. P. Buckley and A. J. Kovacs, Melting Behavior of low Molecular Weight Poly(ethylene-oxide) Fractions 2. Folded Chain Crystals, *Colloid Polym. Sci.*, 1976, **254**, 695–715.
41 L. J. Fetters, D. J. Lohse, D. Richter, T. A. Witten and A. Zirkel, Connection Between Polymer Molecular Weight, Density, Chain Dimensions and Melt Viscoelastic Properties, *Macromolecules*, 1994, **27**, 4639–4647.
42 G. Strobl and G. Colloquium, Laws Controlling Crystallization and Melting in Bulk Polymers, *Rev. Mod. Phys.*, 2009, **81**, 1287–1300.
43 J. Hoffman, G. Davis and J. Lauritzen, in *Treatise on Solid State Chemistry*, ed. N. B. Hannay, Plenum, New York, 1976, vol. 3.
44 S. Rastogi, A. B. Spoelstra, J. G. P. Goossens and P. J. Lemstra, Chain Mobility in Polymer Systems: on the Broadening between Solid and Melt. 1. Lamellar Doubling during Annealing of Polyethylene, *Macromolecules*, 1997, **30**, 7880–7889.
45 A. J. Kovacs, C. Straupe and A. Gonthier, Isothermal Growth, Thickening, and Melting of Poly(ethylene oxide) Single Crystals in the Bulk, *J. Polym. Sci., Polym. Symp.*, 1977, **59**, 31–54.
46 G. Zardalidis and G. Floudas, Pressure effects on the Dynamic Heterogeneity of Miscible Poly(vinylacetate)/Poly(ethylene oxide) Blends, *Macromolecules*, 2012, **45**, 6272–6280.

47 X. Jin, S. Zhang and J. Runt, Observation of a Fast Dielectric Relaxation in Semi-crystalline Poly(ethylene oxide), *Polymer*, 2002, **43**, 6247–6254.
48 G. Floudas, P. Placke, P. Štěpánek, W. Brown, G. Fytas and K. L. Ngai, Dynamics of the ''Strong'' Polymer of n-Lauryl Methacrylate Below and Above the Glass Transition, *Macromolecules*, 1995, **28**, 6799–6807.
49 K. Kunal, C. G. Robertson, S. Pawlus, S. F. Hahn and A. P. Sokolov, Role of Chemical Structure in Fragility of Polymers: a Qualitative Picture, *Macromolecules*, 2008, **41**, 7232–7238.

